

# Anomalous Transport induced by Sheath Instability in Hall Effect Thrusters

IEPC-2009-139

*Presented at the 31st International Electric Propulsion Conference,  
University of Michigan • Ann Arbor, Michigan • USA  
September 20 – 24, 2009*

Francesco Taccogna\* and Pierpaolo Minelli†  
*Istituto di Metodologie Inorganiche e dei Plasmi-CNR, via Amendola 122/D, 70126 Bari, Italy*

Savino Longo‡ and Mario Capitelli#  
*Dipartimento di Chimica, Università degli Studi di Bari, via Orabona 4, 70120 Bari, Italy*

and

Ralf Schneider§  
*Max Planck Institute für Plasmaphysik, Wendelsteinstrasse 1, D-17491 Greifswald, Germany*

**It is well recognized to ascribe the anomalous cross-field conductivity inside Hall-effect thrusters to fluctuation-induced transport due to gradient-driven instabilities (Rayleigh or electron drift) and to electron-wall interaction (near-wall conductivity). In this contribution we have performed a 2D( $r,\theta$ ) Particle-in-Cell (PIC) model showing the possibility of another mechanism inducing azimuthal fluctuations: the lateral sheath instability. It is created by a negative differential resistance of the current-voltage  $I$ - $V$  characteristic of the floating wall as a consequence of high secondary electron emission. Azimuthal modes characterized by frequencies multiplies of  $\nu_0=3$  GHz and a wave number  $k_0=80$  rad<sup>-1</sup> have been detected. By means of a 2D( $\theta,z$ ) Test-Particle Monte Carlo (TPMC) simulation and using the characteristic azimuthal oscillations found in the previous PIC simulation, we have assessed the induced anomalous transport. The contribution calculated is in good agreement the electron cross-field conductivity measured in the acceleration region.**

## Nomenclature

$B$	=	magnetic field
$D$	=	diffusion coefficient
$e$	=	elementary charge
$E$	=	electric field
$k$	=	wave number
$k_B$	=	Boltzmann's constant
$I$	=	current
$m$	=	electron mass

---

\* Researcher, Istituto di Metodologie Inorganiche e dei Plasmi, Consiglio Nazionale delle Ricerche, [francesco.taccogna@ba.imip.cnr.it](mailto:francesco.taccogna@ba.imip.cnr.it).

† Researcher, Istituto di Metodologie Inorganiche e dei Plasmi, Consiglio Nazionale delle Ricerche, [Pierpaolo.minelli@ba.imip.cnr.it](mailto:Pierpaolo.minelli@ba.imip.cnr.it).

‡ Full professor, Dipartimento di Chimica, Università degli Studi di Bari, [savino.longo@ba.imip.cnr.it](mailto:savino.longo@ba.imip.cnr.it).

# Full professor, Dipartimento di Chimica, Università degli Studi di Bari, [mario.capitelli@ba.imip.cnr.it](mailto:mario.capitelli@ba.imip.cnr.it).

§ Head of the Helmholtz-Assoc. Junior Res. Group 'Computational Material Science', [ralf.schneider@ipp.mpg.de](mailto:ralf.schneider@ipp.mpg.de).

$M$	= ion mass
$n$	= particle density
$r$	= radial coordinate
$r_L$	= electron Larmor radius
$r_{in}$	= inner radius (3 cm)
$r_{out}$	= outer radius (5 cm)
$S$	= lateral wall area
$T$	= temperature
$v$	= velocity
$z$	= axial coordinate
$\beta$	= Hall parameter
$\chi$	= critical parameter
$\epsilon_0$	= vacuum permittivity
$\phi$	= electric potential
$\Gamma$	= secondary electron emission coefficient
$\eta$	= azimuthal coordinate
$\mu$	= mobility coefficient
$\nu$	= frequency
$\theta$	= azimuthal coordinate
$\sigma$	= electron conductivity; surface charge density
$\omega$	= angular frequency
$\Omega$	= Larmor frequency

## I. Introduction

One of the fundamental problems in Hall effect thruster discharge concerns the so-called electron *anomalous* transport across the quasi-radial magnetic field<sup>1</sup>. Measurements have established that the axial electron current ( $I_{z,e} \approx 3$  A) is significantly higher than predicted by classical theory ( $I_{z,e,clas} \approx 10^{-1}$  A) due to volumetric collisions. The reason for the observed enhanced cross-field transport is nowadays a subject of considerable and continued debate. However, it is well accepted to mainly attribute the anomalous electron cross-field transport to two different reasons:

- fluctuation-induced transport: anomalous axial electron current results from the correlation between azimuthal electric field  $E_\theta$  and density fluctuations. The origins of these high frequency fluctuations are axial gradient-driven instabilities (Rayleigh-type<sup>2</sup> or electron drift instabilities<sup>3</sup>). This is known to yield a Bohm-type electron cross-field conductivity varying like  $\mu_\perp \sim 1/B$ ;
- wall-induced transport (the so called near-wall conductivity<sup>1</sup>): the electron-wall interactions lead to a non-specular reflection or emission of electrons which leave the walls following another spiral trajectory with the guiding center displaced towards the anode. This yields an electron cross-field conductivity that varies like  $\mu_\perp \sim 1/B^2$ , similarly to classical conductivity due to electron-atom collisions.

Recently<sup>4</sup>, it has been suggested that only the plasma azimuthal fluctuations are responsible for anomalous transport inside and outside the Hall thruster channel. Nevertheless, there is evidence that changing the wall material of Hall thrusters results in significant changes of the electron axial current<sup>5</sup>. In fact, the presence of a high secondary electron emitter as wall material (BN) has a profound effect on the plasma within the Hall channel. Under a moderate emission of secondary electrons from a floating wall, the voltage sheath drop  $\Delta\phi_{sheath}$  is given by<sup>6</sup>:

$$\Delta\phi_{sheath} = -\frac{k_B T_e}{e} \ln \left[ (1 - \Gamma) \sqrt{\frac{M}{2\pi m}} \right] \quad (1)$$

where  $\Gamma = I_{e,s}/I_{e,p}$  is the ratio between primary electron current impacting on the wall and the secondary electron current emitted from the wall, is the secondary electron emission coefficient. It is a function of the energy and angle of impact. The electrons in the Hall discharge have energies in the range of 15-20 eV (energy range necessary to ionize Xenon). Due to their azimuthal  $v_d = \mathbf{E} \times \mathbf{B}$  drift and after passing the retarding sheath drop they impact the walls under grazing incidence. These circumstances make the classical Debye layer to disappear and to transform (if  $\Gamma \approx 1 - 8.3\sqrt{m/M}$ <sup>6</sup>) into a non-monotonic behavior (double layer structure). A potential well forms close to the

wall, which traps a fraction of the secondary electrons (space charge saturation regime). This theory is based on the assumption that the zero total current condition at the wall is statically fulfilled:

$$I_i = -I_{e,tot} = I_{e,p} + I_{e,s} = I_{e,p}(1 - \Gamma) \quad (2)$$

(note that the emission of secondary electrons produces a positive current). In fact, if  $I_i$  increases, the floating potential of the wall increases and the voltage sheath drops decreases in order to enhance the primary electron flow  $I_{e,p}$  (dominant in the total electron current). But if  $\Gamma$  exceeds 1 the sheath loses its static character becoming an oscillating structure, the so-called sheath instability<sup>7-10</sup>. This is due to the appearance of a negative differential resistance in the  $I$ - $V$  characteristics of the wall  $(\partial I/\partial V)^{-1} < 0$ . If  $I_i$  increases in this case, then the voltage sheath drop cannot decrease, because otherwise the primary electrons would strike the wall with higher energy creating a higher emission current of secondary electrons  $I_{e,s}$ , which would increase the positive current. The importance of the sheath instability is also supported by the observed so-called anomalous erosion structure<sup>1</sup>.

The apparently contrasting evidence that on one hand anomalous transport inside Hall thrusters is fluctuation-induced and that on the other hand wall material changes the electron axial current are both confirmed within one model in the present contribution, where we report results from numerical experiments demonstrating the presence of azimuthal fluctuations induced by the sheath instability.

## II. Numerical Model

We concentrate our efforts in the study of the dynamics of electrons in a  $(r, \theta)$  plane, neglecting all the axial pressure (density and/or temperature) gradients. The axial location investigated is the acceleration region of the thruster, where, a large drift velocity is responsible for the secondary electron emission instability. Indeed, experimental measurements<sup>18</sup> show in this region a pronounced deviation of the inverse Hall parameter  $\beta^{-1} = j_{e,z}/j_{e,\theta}$  (quantity directly related to the cross-field mobility  $\beta^{-1} = \mu_{\perp} B$ ) from both the classical and Bohm value (see Fig. 1):

$$\frac{\beta_{coll}}{1 + \beta_{coll}^2} < \frac{1}{\beta_{eff}} < \frac{1}{16}, \quad (3)$$

where  $\beta_{coll} = \Omega/\nu_{eN}$  represents the number of cyclotron rotation which an average electron may complete between momentum transfer collisions.

With the azimuthal fluctuation characterization, a Test-Particle Monte Carlo technique in a  $(\theta, z)$  plane has been developed in order to assess the induced anomalous transport.

### A. 2D( $r, \theta$ ) Particle-in-Cell / Monte Carlo electrostatic model

The numerical model consists of a fully kinetic electrostatic Particle-in-Cell/Monte Carlo Collision (PIC-MCC) simulation<sup>11</sup>. In order to correlate the radial and

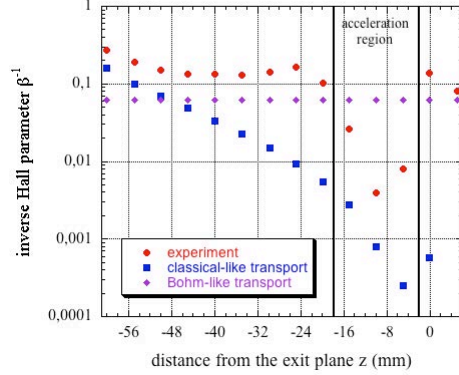
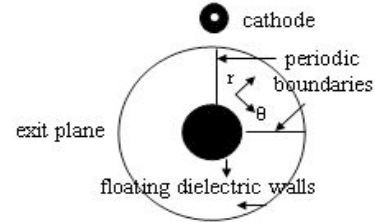
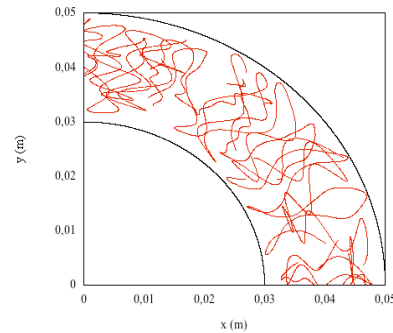


**Figure 1. Inverse of the Hall parameter vs the axial position (from [18]).**



(a)



(b)

**Figure 2. (a) Sketch of the 2D( $r, \theta$ ) simulation domain. (b) Trajectories of electrons inside the simulation domain.**

azimuthal dynamics, a two-dimensional  $(r, \theta)$  domain is investigated. It consists of a cross section of the exhaust region of the annular channel (see Fig. 2). To exclude the contribution of axial gradients as possible causes of the azimuthal fluctuations we use by purpose this reduced model, where uniformity in axial direction is explicitly chosen. Indeed, in this part of the channel, the electron radial and azimuthal dynamics are much faster than the axial one due to the radial magnetic field impedance. We are aware of the fact that in the real system also turbulence driven by axial gradients will exist. However, this model system gives the possibility to check the existence of surface-driven turbulence without interference with other types of turbulence. Secondary electron emission is self-consistently taken into account by means of a detailed probabilistic Monte Carlo model<sup>12,13</sup>. The simulation is initiated with a uniform homogeneous distribution of Maxwellian macro-particles (electrons and Xe<sup>+</sup>), using as input parameters:

- neutral density  $n_N = 2 \times 10^{18} \text{ m}^{-3}$ ;
- axial electric field  $E_z = 2 \times 10^4 \text{ V/m}$ ;
- radial magnetic field  $B_{r, in} = 150 \text{ Gauss}$ .

The radial variation of  $n_N$  and  $E_z$  is considered to be negligible, while the radial component of  $B$  is written as  $B_r(r) = B_{r, in} r_{in} / r$ , in order to fulfill the divergence free  $\nabla \cdot \mathbf{B} = 0$  condition in cylindrical metric. A von-Neumann condition is used on the insulating walls: the electric field at the wall is normal to the surface and proportional to the net charge  $\sigma(\theta, t)$  accumulated on the surface in each cell (the possible surface conductivity of the dielectric is neglected in comparison to the plasma conductivity):

$$\left. \frac{\partial \phi_{wall}(\theta, t)}{\partial r} \right|_w = -\frac{1}{\epsilon_0 S} \int_0^t [I_i(\theta, t') + I_{e,p}(\theta, t')(1 - \Gamma(\theta, t'))] dt', \quad (4)$$

while periodic boundary conditions are set on the azimuthal boundaries. The discharge is sustained with electrons created by bulk ionization (electron-neutral elastic collision and excitation are also included) and surface emission and injected (simulating the cathode neutralizer) in order to preserve the global neutrality of the system. Complementary features of the model are presented in Ref. [14].

## B. 2D( $\theta, z$ ) Test-Particle Monte Carlo transport model

In the second model, we neglect the radial dynamics and we focus our attention on the  $(z, \theta)$  plane using a fixed oscillating azimuthal field with characteristics (the most dominant frequencies and wave numbers) found in the previous model. We consider a collection of particles having a little action on wave, considering them as test particles subjected to it. Neglecting the radial coordinate, the near-wall conductivity contribution is nullified. Furthermore, electron-neutral collision processes are switched off in order to avoid the transport coming from the classical contribution as well.  $5 \times 10^6$  electron orbits are tracked with the initial velocity condition sampled from a Maxwellian distribution with  $T_e = 5 \text{ eV}$ . This last assumption makes also possible to avoid the contribution to cross-mobility coming from a non-equilibrium distribution function<sup>15</sup>:

$$\mu_{\perp} = \frac{4}{3} \pi \frac{e}{m} \int_0^{\infty} v^3 \frac{v}{v^2 + \Omega^2} \left( -\frac{\partial f}{\partial v} \right) dv \quad (5)$$

This part of the work represents the theory of Hamiltonian maps and chaos in dynamical systems<sup>16</sup>. The analysis of a particle dynamics in the field of a wave packet propagating along  $\theta$ .

$$E_{\theta} = \sum_k E_k \cos(k\theta - \omega_k t) \quad (6)$$

with an imposed transverse magnetic field  $B_r$  has been exhaustively studied, due to the fact that it has a broad range of applications, among them stochastic plasma heating and acceleration, bounce-resonances in the magnetosphere, etc. It leads to the study of the motion of a linear oscillator in a travelling wave field (known as kicked rotor):

$$\ddot{\eta} + \Omega^2 \eta = \sum_k \chi_k \cos[k(\eta + \theta_{gc}) - (\omega_k - kv_d)t] \quad (7.a)$$

$$\dot{z} = \Omega(\eta + \theta_{gc}) \quad (7.b)$$

where  $\eta = \theta - v_d t - \theta_{gc}$  (referential system moving with the guiding center  $gc$  along the azimuthal direction  $\theta$  with the drift velocity  $v_d$ ),  $\Omega$  is the Larmor frequency and  $\chi_k = \Omega v_d E_k / E_z$  is the critical parameter.

Under certain circumstances, it has been proven<sup>17</sup> that the regular motion can become stochastic

$$\frac{E_k}{E_z} > \frac{1}{4} \left( \frac{\Omega}{k v_d} \right)^{1/3} \quad (8)$$

and for high frequency ( $\omega_k > \Omega$ ) the quasi-linear approach is no more valid (nonlinear effect of trapping). In fact, in this case the perturbation acts on the circumferential angular motion of the electron changing substantially the particle trajectory.

The electron (with its cyclotron motion) and the wave exchange most energy while in the resonance, that is when the azimuthal component of the electron velocity  $\dot{\eta}$  is close to the phase velocity of the wave:

$$v_\phi = \frac{\omega_k - k v_d}{k}. \quad (9)$$

The particle receives a kick from the wave (wave-particle virtual collision), while between two kicks the electron trajectory remains close to a drifting cyclotron orbit (epitrochoidal curve). The orbit does not return to the same  $\eta$  since the kick pushes the particle in the negative  $\eta$  direction and hence it produces an increment of the axial speed [see eq. (7.b)].

It has to be pointed out that due to the resonance nature of the anomalous transport, the Spitzer<sup>19</sup> and Yoshikawa-Rose<sup>20</sup> theories (valid for  $k \ll r_L^{-1}$  and  $\omega_k \ll \Omega$ ) are not applicable.

### III. Results

#### A. Azimuthal oscillations driven by sheath instability

This section shows results obtained by the first model. Fig. 3 shows the temporal evolution of the radial (black line) and azimuthal (red line) average drift energy of the electron system  $E_{d,r} = \frac{1}{2} m \langle v_{e,r}^2 \rangle$

and  $E_{d,\theta} = \frac{1}{2} m \langle v_{e,\theta}^2 \rangle$ , where averaging  $\langle \dots \rangle$  is

performed over the complete electron ensemble. Two jumps are evident occurring at  $t = 3.7 \times 10^{-7}$  s and  $t = 8.4 \times 10^{-7}$  s, when the sheath instability develops as the differential resistance in the  $I$ - $V$  characteristics of the wall  $(\partial I / \partial V)^{-1}$  becomes negative. Before and after these jumps, the energy oscillation amplitude is relatively small. When the fluctuation in the radial energy appears, the azimuthal drift energy starts to fluctuate as well. As a confirmation of this sequence, Fig. 4 shows the azimuthal profile (between 0 and  $\pi/16$ ) of  $E_\theta$  at three different times: before the first instability (full line) and during the first

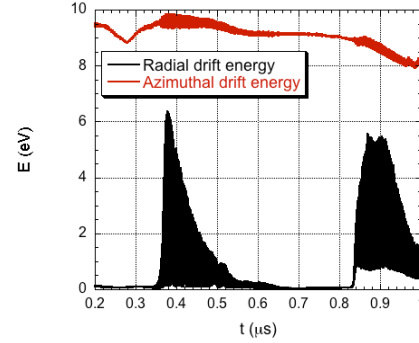


Figure 3. Time history plot of the radial (black line) and azimuthal (red line) average drift energy of the electron system.

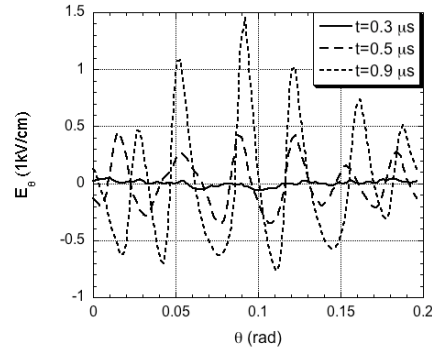


Figure 4. Azimuthal profile (between 0 and  $\pi/16$ ) of the azimuthal component of the electric field  $E_\theta$  at three different times: a)  $t = 3 \times 10^{-7}$  s, before the first instability (full line); b)  $t = 5 \times 10^{-7}$  s, during the first instability (dashed line); c)  $t = 9 \times 10^{-7}$  s, during the second instability (dotted line).

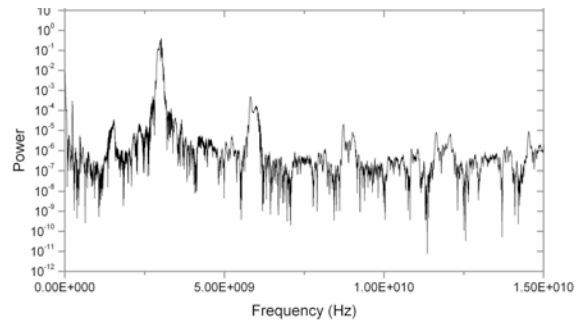


Figure 5. Power spectra of the potential oscillation detected at a single point  $(r, \theta) = (0.04 \text{ m}, 0.1 \text{ rad})$ .

and the second instability (broken lines). The fluctuating structure starts to appear during the first instability (when  $|E_\theta| \sim E_z$ ) and the amplitude of the fluctuation increases during the second instability (when  $|E_\theta| \sim 5E_z$ ). The sheath radial instability works as trigger condition for the azimuthal fluctuation. It modulates the electron azimuthal beam, causing charge imbalances. These in turn create an oscillating azimuthal electric field, which propagates with a wavelength

$$\lambda_\theta = \frac{v_d}{v_{si}} \quad (10)$$

where  $v_{si}$  is the frequency of the sheath instability. From the numerical experiment we have found the presence of different frequencies multiple of a fundamental one  $\nu_0=3$  GHz (see Fig. 5), giving from eq. (10) a wavelength  $\lambda_\theta=0.45 \times 10^{-3}$  m (corresponding to a wave number  $k_\theta=80$   $\text{rad}^{-1}$ ).

In Fig. 6 the temporal evolution of the total current  $I_{\text{tot}}$  collected on the outer wall and the corresponding floating potential  $\phi_{\text{wall}}$  (integrated over the entire azimuthal domain) as result from eq. (4) is shown. Actually, the instability is detected only on the outer wall, where the secondary electron emission coefficient reaches a value larger than 1,  $\Gamma=1.295$ , while in the inner wall  $\Gamma=0.992$ . The most likely reason for this difference between the two walls is due to a magnetic mirror effect as a consequence of the  $1/r$  variation of the magnetic field.

## B. Axial electron anomalous transport induced

This section shows results obtained by the second model. The electron transport across the magnetic field is measured for a set of test particles averaging the axial position of the guiding centers on the ensemble of electrons. For an electron in a magnetic field it is given by:

$$z_{gc} = z - \frac{\dot{\theta}}{\Omega}. \quad (11)$$

The guiding center of the particles does not show the rapid oscillatory motion that the particle positions exhibit. They are therefore suitable for computation of mobility across the magnetic field. Fig. 7 shows the temporal evolution of  $\langle z_{gc} \rangle$ . A drift towards the anode ( $z > 0$ ) is evident originating from the azimuthal field (6) imposed. Without collisions and anomalous transport, the average axial position of the guiding centers should have a constant value equal to the initial condition. Fig. 7 shows also the resonant nature of the axial transport. The resulting anomalous electron axial mobility  $\mu_z = v_z / E_z$  induced just by the sheath instability is calculated to be  $\mu_z = 0.25 \text{ m}^2/\text{Vs}$  (corresponding to an inverse Hall parameter  $\beta^{-1} = 3.8 \times 10^{-3}$ ), which is in good agreement with the experimental value<sup>18</sup> measured in the exhaust region of the annular channel (see

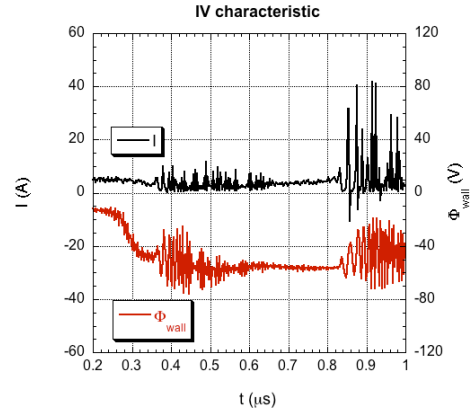


**Figure 6. Temporal evolution of current-voltage I-V characteristic of the outer wall. The total current  $I_{\text{tot}}$  collected on the outer wall and the corresponding floating potential  $\phi_{\text{wall}}$  [as result from eq. (4)] are integrated over the entire azimuthal domain.**

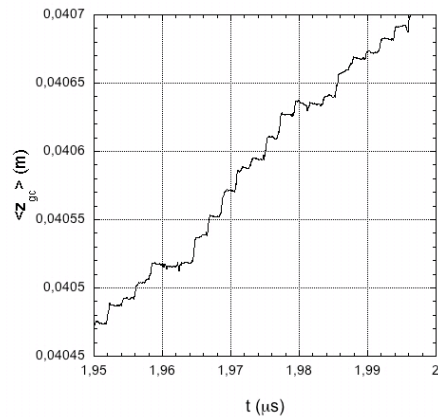


**Figure 7. Time evolution of the averaged value of the axial coordinate of the guiding center.**

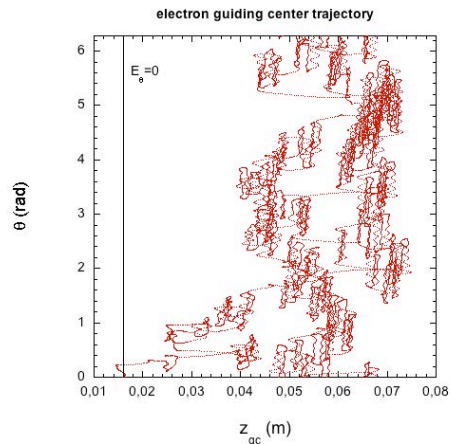


**Figure 8. Temporal evolution (2  $\mu\text{s}$ ) of the point  $(z_{gc}, \theta)$  from left to right side.**

Fig. 1). The experimental value is the result of the contribution coming also from axial-gradient induced, near-wall and classical mobility. However, it has to be pointed out that most likely all the different contributions do not necessarily add each other, but they interfere in non-linear way giving the experimental value.

The resonant nature of the axial electron transport is also evident reported in Fig. 8, where we have plotted the trajectory (the temporal window is 2  $\mu$ s) of the point  $(z_{gc}, \theta)$ . From this figure it is evident the combination of particle trapping in eddies for long times and jumps over several sets of eddies in a single flight leading to anomalous diffusion coming from space and time correlations (interaction between electron dynamics and coherent structures) which gives a non-local in space (non-Gaussian) and time (non-Markovian) transport.

#### IV. Conclusion

The present PIC model has shown that fluctuation-induced anomalous transport inside the Hall effect thruster discharge can also be related to the sheath instability and not only to the gradient-driven instabilities. In fact, a high frequency sheath instability has been detected due to the appearance of a negative differential resistance in the  $I$ - $V$  characteristics of the outer wall. The driving mechanism has been identified as the high secondary electron emission produced by the impact of electrons from the  $\mathbf{E} \times \mathbf{B}$  azimuthal flow. The model predicts the presence of purely azimuthal modes in the discharge characterized by a frequencies multipliis of  $\nu_0=3$  GHz and a wave number of  $k_\theta=80$  rad $^{-1}$ . By means of a Test-Particle Monte Carlo simulation and using the characteristic azimuthal oscillation found in the previous PIC simulation, we have assessed the anomalous transport induced which is in good agreement with the experimental measurement. Future numerical 3D works will enable us to evaluate the other different contributions and to understand the interaction among them in order to identify the leading mechanism inducing the total anomalous transport.

#### Acknowledgments

This work was supported by the Italian Minister for University and Research (MIUR) under the contract MIUR-PRIN 2008: “Dinamica dei processi elementari per la chimica e la fisica dei plasmi”. R. Schneider acknowledges funding of the work by the Initiative and Networking Fund of the Helmholtz Association.

#### References

- <sup>1</sup>Morozov, A. I., and Savel'ev, V. V., *Reviews of Plasma Physics* Vol. 21, ed. B. B. Kadomtsev and V. D. Shafranov, New York, 2000, pp. 203.
- <sup>2</sup>Litvak, A. A., and Fisch, N. J., *Phys. Plasmas*, Vol. 11, No. 4, pp. 1379, 2004.
- <sup>3</sup>Ducrocq, A., Adam, J. C., Héron, A., and Laval, G., *Phys. Plasmas*, Vol. 13, 102111, 2006.
- <sup>4</sup>Boniface, C., Garrigues, L., Hagelaar, G. J. M., Boeuf, J. P., Gawron, D., and Mazouffre, S., *Appl. Phys. Lett.*, Vol. 89, 161503, 2006.
- <sup>5</sup>Raitses, Y., Smirnov, A., Staack, D., and Fisch, N. J., *Phys. Plasmas*, Vol. 13, 014502, 2006.
- <sup>6</sup>Hobbs, G. D., and Wesson, J. A., *Plasma Phys.*, Vol. 9, pp. 85, 1967.
- <sup>7</sup>Kirdyashev, K. P., *Tech. Phys. Lett.*, Vol. 23, No. 5, pp. 395, 1997.
- <sup>8</sup>Griskey, M. C., and Stenzel, R. L., *Phys. Rev. Lett.*, Vol. 82, No. 3, pp. 556, 1999.
- <sup>9</sup>Morozov, A. I., and Savel'ev, V. V., *Plasma Phys. Rep.* Vol. 33, No. 1, pp. 20, 2007.
- <sup>10</sup>Sydorenko, D., Smolyakov, A., Kaganovich, I., and Raitses, Y., *Phys. Plasmas*, Vol. 15, 053506, 2008.
- <sup>11</sup>Birdsall, C. K., and Langdon, A. B., *Plasma Physics via Computer Simulation*, ed. McGraw-Hill, New York, 1985.
- <sup>12</sup>Furman, M. A., and Pivi, M. T. F., *Phys. Rev. Special Topics-Accel. and Beams* Vol. 5, 124404, 2002.
- <sup>13</sup>Cimino, R., Collins, I. R., Furman, M. A., Pivi, M. T. F., Ruggiero, F., Rumolo, G., and Zimmermann, F., *Phys. Rev. Lett.* Vol. 93, No. 1, 014801, 2004.
- <sup>14</sup>Taccogna, F., Schneider, R., Longo, S., and Capitelli, M., *Plasma Source Sci. & Techn.* Vol. 17, No. 2, 024003, 2008.
- <sup>15</sup>Mitchner, M. Kruger, C. H. Jr., *Partially Ionized Gases*, ed. Wiley and Sons, New York, 1973.
- <sup>16</sup>Sagdeev, R. Z., and Zaslavskii, G. M., in *Nonlinear Phenomena in Plasma Physics and Hydrodynamics*, ed. by R. Z. Sagdeev, MIR Publishers Moscow, 1986.
- <sup>17</sup>Karney, C. F. F. *Phys. Fluids*, Vol. 21, No. 9, pp. 1584, 1978; Vol. 22, No. 11, pp. 2188, 1979.
- <sup>18</sup>Meezan, N. B., Hargus, W. A. Jr., and Cappelli, M. A., *Phys. Rev. E*, Vol. 63, 026410, 2001.
- <sup>19</sup>Spitzer, L. Jr., *Phys. Fluids*, Vol. 3, pp. 659, 1960.
- <sup>20</sup>Yoshikawa, S., and Rose, D., *Phys. Fluids*, Vol. 5, pp. 334, 1962.